Advanced 3D Monte Carlo Algorithms for Biophotonic and Medical Applications

Lewis McMillan

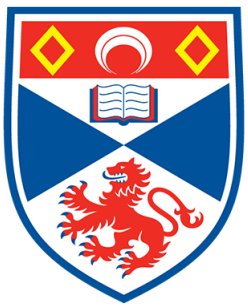

University of
St Andrews

This thesis is submitted in partial fulfilment for the degree of
PhD
at the
University of St Andrews

March 2019

Declaration

I, Lewis McMillan, hereby certify that this thesis, which is approximately ***** words in length, has been written by me, that it is the record of work carried out by me, or principally by myself in collaboration with others as acknowledged, and that it has not been submitted in any previous application for a higher degree.

I was admitted as a research student in September 2015 and as a candidate for the degree of PhD in September 2015; the higher study for which this is a record was carried out in the University of St Andrews between 2015 and 2019.

Date ..... Signature of candidate .....

I hereby certify that the candidate has fulfilled the conditions of the Resolution and Regulations appropriate for the degree of PhD in the University of St Andrews and that the candidate is qualified to submit this thesis in application for that degree.

Date ..... Signature of supervisor .....

Date ..... Signature of supervisor .....

Abstract

Lorem ipsum dolor sit amet, consectetuer adipiscing elit. Ut purus elit, vestibulum ut, placerat ac, adipiscing vitae, felis. Curabitur dictum gravida mauris. Nam arcu libero, nonummy eget, consectetuer id, vulputate a, magna. Donec vehicula augue eu neque. Pellentesque habitant morbi tristique senectus et netus et malesuada fames ac turpis egestas. Mauris ut leo. Cras viverra metus rhoncus sem. Nulla et lectus vestibulum urna fringilla ultrices. Phasellus eu tellus sit amet tortor gravida placerat. Integer sapien est, iaculis in, pretium quis, viverra ac, nunc. Praesent eget sem vel leo ultrices bibendum. Aenean faucibus. Morbi dolor nulla, malesuada eu, pulvinar at, mollis ac, nulla. Curabitur auctor semper nulla. Donec varius orci eget risus. Duis nibh mi, congue eu, accumsan eleifend, sagittis quis, diam. Duis eget orci sit amet orci dignissim rutrum.

Nam dui ligula, fringilla a, euismod sodales, sollicitudin vel, wisi. Morbi auctor lorem non justo. Nam lacus libero, pretium at, lobortis vitae, ultricies et, tellus. Donec aliquet, tortor sed accumsan bibendum, erat ligula aliquet magna, vitae ornare odio metus a mi. Morbi ac orci et nisl hendrerit mollis. Suspendisse ut massa. Cras nec ante. Pellentesque a nulla. Cum sociis natoque penatibus et magnis dis parturient montes, nascetur ridiculus mus. Aliquam tincidunt urna. Nulla ullamcorper vestibulum turpis. Pellentesque cursus luctus mauris.

Acknowledgements

Lorem ipsum dolor sit amet, consectetuer adipiscing elit. Ut purus elit, vestibulum ut, placerat ac, adipiscing vitae, felis. Curabitur dictum gravida mauris. Nam arcu libero, nonummy eget, consectetuer id, vulputate a, magna. Donec vehicula augue eu neque. Pellentesque habitant morbi tristique senectus et netus et malesuada fames ac turpis egestas. Mauris ut leo. Cras viverra metus rhoncus sem. Nulla et lectus vestibulum urna fringilla ultrices. Phasellus eu tellus sit amet tortor gravida placerat. Integer sapien est, iaculis in, pretium quis, viverra ac, nunc. Praesent eget sem vel leo ultrices bibendum. Aenean faucibus. Morbi dolor nulla, malesuada eu, pulvinar at, mollis ac, nulla. Curabitur auctor semper nulla. Donec varius orci eget risus. Duis nibh mi, congue eu, accumsan eleifend, sagittis quis, diam. Duis eget orci sit amet orci dignissim rutrum.

Nam dui ligula, fringilla a, euismod sodales, sollicitudin vel, wisi. Morbi auctor lorem non justo. Nam lacus libero, pretium at, lobortis vitae, ultricies et, tellus. Donec aliquet, tortor sed accumsan bibendum, erat ligula aliquet magna, vitae ornare odio metus a mi. Morbi ac orci et nisl hendrerit mollis. Suspendisse ut massa. Cras nec ante. Pellentesque a nulla. Cum sociis natoque penatibus et magnis dis parturient montes, nascetur ridiculus mus. Aliquam tincidunt urna. Nulla ullamcorper vestibulum turpis. Pellentesque cursus luctus mauris.

Contents

Abbreviations

MCRT Monte Carlo radiation transfer.

NM Nelder-Mead.

List of Figures

Chapter 1

AmoebaMCRT, modelling autofluorescence in skin for novel biomarkers of cardiovascular disease

1.1 Introduction

1.2 Skin Model

So far in this thesis all tissue models have been simplified, by assuming that tissue is a homogeneous structure with uniform optical properties. However this is not the case in reality. Tissue is very un-homogeneous, with non-uniform optical properties. However to create a 1 to 1 model of tissue in a simulation is impractical due to the resolution required to resolve all the constituent part of the tissue down to the cell level. Therefore we need to make a compromise between reality and what is possible to model efficiently. To this end the section presents a 5 layer model of human skin. Dermatologists usually split the skin into 5 layers: Stratum Corneum, Epidermis*, Papillary Dermis, Reticular Dermis, and Hypodermis, see Fig. 1.1.

Each of these layers have various amounts of chromophores and scatterers. To accurately model these various chromophores and scatterers, and therefore the skin, we must discuss the chemical makeup and spatial structure of the skin.

Stratum Corenum

The top most layer of the skin is the stratum corenum. This layer mostly consists of dead skin cells (keratinocytes). The function of this layer is to be a protection barrier to prevent damage, infection and diffusion of unwanted chemicals.

*The epidermis can be split into several more layers, however these layers are optical similar and are rather small so we model just one layer here.

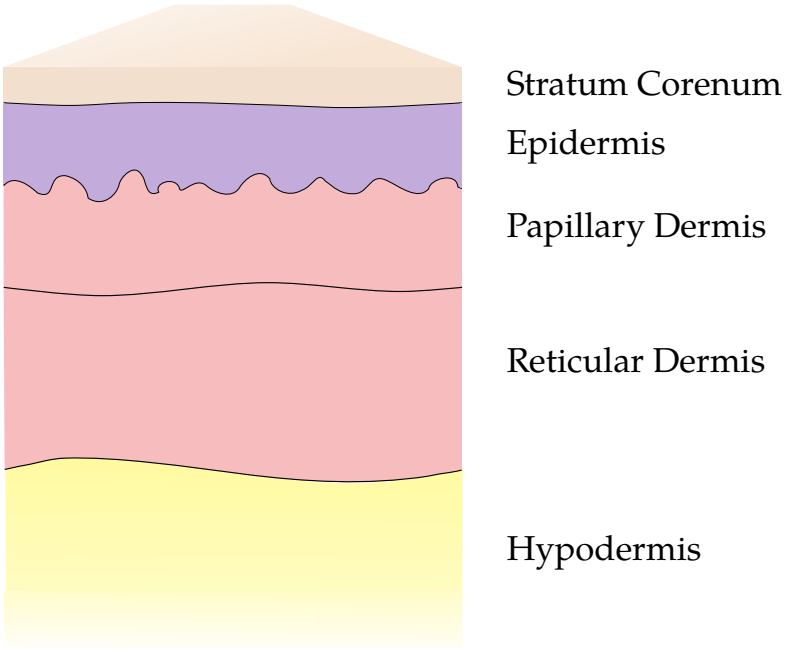

Figure 1.1: *Illustration of skin layers in human skin.*

Epidermis

Below the stratum corenum is the epidermis. The epidermis consist of several layers that are optically similar so we restrict out model to modelling as one whole layer. The layers that make up the epidermis are the stratum basale, stratum spinosum, stratum granulosum, and the stratum lucidum[†]. The purpose of the epidermis is as before to provide a protective barrier to the underlying layers. The epidermis contains melanin which protects the stem cell keratinocyte which divide to form keratinocyte which form much of the upper layers of the skin. In the stratum basale there is also melanocyte which produce the pigment melanin which is responsible for the color of the skin, and providing some protection from harmful UV light. Other types of cells found i the epidermis are Langerhans cells and Merkel cells which are part of the immune system and nervous system respectively.

Dermis

The dermis is split into three different layers in our model: the papillary dermis, reticular dermis and the hypodermis.

The papillary dermis has blood

The reticular dermis has blood

The hypodermis consists of fat and

[†]The stratum corenum is usually part of the epidermis, however as its optical properties are different than that of the epidermis we model it as a separate layer.

Optical Properties

With a discussion of what makes up the skin, and what molecules contribute to the skins optical properties, this section gives an account of how our skin model, models the optical properties of skin.

To model blood, we first split blood into Deoxygenated and Oxygenated. We mix these two groups using the tissue oxygenation coefficient S. Blood absorption spectra are taken from

$$\mu_{a,oxy/deoxy} = 150 \ \ln 10 \ \frac{\epsilon}{64458} \tag{1.1}$$

$$\mu_{a,b}(\lambda) = SO_2\mu_{a,Oxy} + (1 - SO_2)\mu_{a,DeOxy} \tag{1.2}$$

The next chromophores are bilirubin and β-carotene. The absorption coefficients are calculated using the blah

$$\mu_{a,Bilirubin}(\lambda) = \frac{\epsilon_{bilirubin}}{585} \ ln10 \ C_{bilirubin} \tag{1.3}$$

$$\mu_{a,\beta-Caro}(\lambda) = \frac{\epsilon_{\beta-Caro}}{537} \ ln10 \ C_{\beta-Caro} \tag{1.4}$$

To model melanin‘’s absorption coefficient we use Eq. (1.5), taken from...

$$\mu_{a,mel}(\lambda) = 6.66 \times 10^{11} \times \lambda^{-3.33} \tag{1.5}$$

Finally we use a base absorption coefficient to model the absorption due to the other parts of the skin that contribute to its optical properties, but individually do not have a large effect.

$$\mu_{a,b} = 7.84 \times 10^{8} \times \lambda^{-3.255} \tag{1.6}$$

Figure 1.2: *Absorption coefficients for the various chromophores found in skin.*

1.3 Modelling Fluorescence

Fluroescene is the process in which light of a certain wavelength is incident on a molecule, the molecule absorbs the light and re-emits the light at a new longer wavelength.

Figure 1.3 shows an example of Jablonski diagram.

To model fluorescence from multiple fluorophores requires a change of the Monte Carlo radiation transfer (MCRT) code presented thus far. This change is to the interaction portion of the algorithm, so that it will now include the option for a packet to undergo fluorescence. To calculate whether a packet absorbs, scatters or fluoresces, first the probability of each of these events must be calculated. Discussion of scattering and absorption (by the bulk medium) was described in **??**. To calculate the probability of fluorescence, we first assume that the quantum yield of the molecule is unity. This is physically unrealistic, however it does not affect the simulations accuracy, as modelling a realistic quantum yield would mean that more packets would be discarded, and thus the signal to noise ration would be worse than if we assume a quantum yield of unity. To calculate the probability of fluorescence, the absorption coefficient of the florescent molecule must be calculated. This is shown in Eq. (1.7):

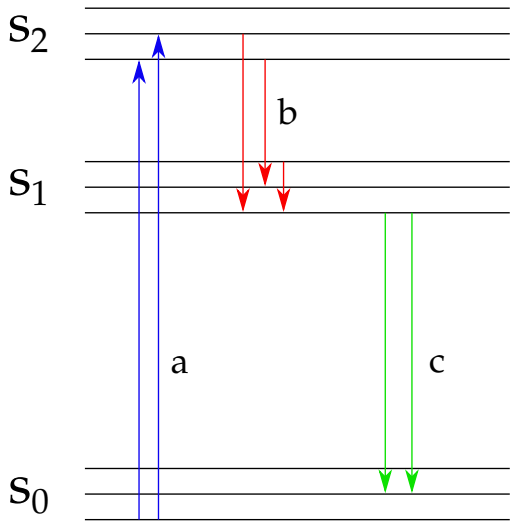

Figure 1.3: *Jablonski diagram for PPIX. a) excitation of the ground state via absorption of a photon, b) non-radiative transition, and c) fluorescence.*

$$\mu_f = \ln(10)\, C\varepsilon \tag{1.7}$$

Where C is the concentration of the fluorophore, ε is the extinction coefficient of the fluorophore, and $ln(10)$ is the natural logarithm of 10[‡].

The next step is to calculate the total attenuation coefficient for a given species as in Eq. (1.8)

$$\mu_{t_i} = \mu_{s_i} + \mu_{a_i} + \mu_{f_i} \tag{1.8}$$

Where as usual μ_a and μ_s are the absorption and scattering coefficients, and μ_f is the fluorescence coefficient as defined in Eq. (1.7). As the absorption coefficient of fluorophores are small in comparison to the medium, and that the absorption coefficient of fluorescent molecules are generally much larger than that of their scattering coefficient, we assume that the scattering coefficient is negligible. Finally we calculate the probability of interacting with a given species using Eq. (1.9)

$$P_i = \frac{\mu_{t,i}}{\sum_{i=1}^{N} \mu_{t,i}} \tag{1.9}$$

Where P_i is the probability of interacting with the i^{th} species, the numerator is the attenuation coefficient for i^{th} species, and the denominator is the total attenuation coefficient for all the species.

Algorithm 1 shows the process used to determine which species to interact with.

[‡]This factor appears as historically ε was measured in base 10 [1].

```
set μ_tot;
set all P_i's;
set ξ_1;
if ξ_1 < P_1 then
    set ξ_2;
    if ξ_2 < a_m then
        Scatter in medium;
    else
        Absorb in medium;
    end
else if ξ_1 < P_1 + P_2 then
    Species 1 fluoresces;
else if ξ_1 < P_1 + P_2 + P_3 then
    Species 2 fluoresces;
else if ξ_1 < P_1 + P_2 + P_3 + ... + P_n then
    Species n fluoresces;
else
    Error;
end
```

Algorithm 1: *An algorithm to determine which species to interact with. P_1 is the probability of interacting with the bulk medium, P_2 to P_n is the probability of interacting with a fluorescent species, a_m is the albedo of the bulk medium, ξ_i is a random number, and μ_{tot} is the total attenuation coefficient of all the species summed.*

This method allows an arbitrary number of fluorophores to be modelled.

1.4 Nelder-Mead Method

The Nelder-Mead (NM) method is an algorithm for unconstrained optimisation. The algorithm is based upon iteratively updating a simplex. A simplex is a structure in $n-dimensional$ space, consisting of $n+1$ points that are not in the same plane. Therefore in 1D, the simplex is a line, in 2D a triangle, in 3D a tetrahedron, etc.. The Nelder-Mead method is a gradient free method, meaning that it does not require derivatives to be calculated and that the search space does not need to be smooth. This makes it ideal for problems where derivates are not able to be computed easily, or the search space is not smooth. However the NM method can also get stuck at local minima so care must be taken to avoid this.

The NM algorithm works by removing the worst vertex of the simplex and replacing it with a 'better' vertex calculated via a number of different operations. These operations can be seen in Fig. 1.4.

The first step of the NM method is to sort the initial vertices according to their fitness. For $n = 2$, we define x_w as the 'worst' point, x_l and the 'lousy' point, and x_b the 'best' point, such that $f(x_b) \leq f(x_l) \leq f(x_w)$, where $f(x)$ is evaluating the 'fitness' of a point x. The fitness function varies from problem to problem, and usually takes the form of the function that is being optimised.

With the vertices sorted, the centroid of the simplex is calculated as in Eq. (1.10). The centroid is the mean of all the vertices bar the 'worst' point.

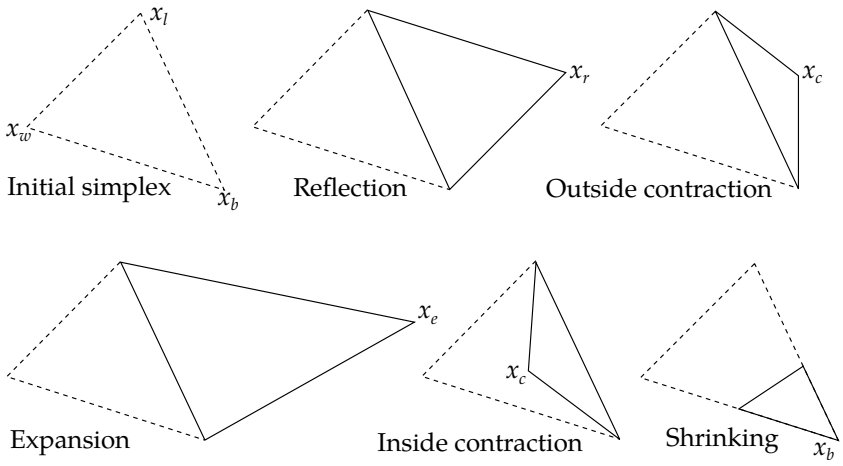

Figure 1.4: *Operations that can be preformed on a simplex for $n = 2$.*

The next step is to move the simplex via a reflection. To calculate the new vertex via reflection Eq. (1.11) is used, where α is the reflection factor. If this new point, x_r, is better[§] than the current 'best' point then we calculate a new point in the same direction but further using the expansion operation Eq. (1.12), where γ is the expansion factor. If this new point, x_e, is better than the 'best' point then we replace x_w with x_e and start the process again. However is x_e is not better than the 'best' point, then we discard it and replace the worst point with x_r the reflected point.

If when calculating x_r, we find that is worse than the 'best' point, we then check if x_r is better than the 'lousy' point. If x_r is better than x_l then we replace the 'worst' point and start the process again. However if the x_r is worse than x_l, we then compare it to the 'worst' point. If x_r is better than the 'worst' point then we preform and inside contraction Eq. (1.14), where β is the contraction factor. If this new point, x_{ic}, is better than the 'worst' point then we keep it, otherwise we preform the shrink operation, shrinking the whole simplex around the 'best' point.

If x_r is not worse than the 'worst' point then we preform an outside contraction Eq. (1.13). This computes a new point x_{oc}. If x_{oc} is better than x_w, then we keep it, otherwise again we shrink around the 'best' point.

The process described above is summarised in Fig. 1.5. Standard values for the factors are: $\alpha = 1$, $\beta = \frac{1}{2}$, and $\gamma = 2$. Though in practice these values are adjusted for the problem at hand.

$$c = \frac{1}{n} \sum_{i=1, i \neq w}^{n+1} x_i \tag{1.10}$$

$$x_r = c + \alpha(c - x_w) \tag{1.11}$$

$$x_e = c + \gamma(x_r - c) \tag{1.12}$$

$$x_{oc} = c + \beta(x_r - c) \tag{1.13}$$

$$x_{ic} = c + \beta(x_w - c) \tag{1.14}$$

As the Nelder-Mead method has no inbuilt convergence criteria, this must be added. We use two different criteria based upon simplex size, and vertex fitness. The criteria for the simplex

[§]Here better means the point has a lower fitness score

size is as; The size of the simplex is calculated using Eq. (1.15):

$$size = \sum_{i=1}^{n+1} |p_i - p_{i+1}| \tag{1.15}$$

Where p_i and p_{i+1} are vertices in the simplex that are connected by an edge. If the size of the simplex falls below a pre-set value, then we preform a factorial test to see if the simplex should be restarted or if the algorithm should terminate. The factorial test checks the space around the current simplex to ensure that we have converged to a global minima. If the check fails then the algorithm is restarted with the current best point kept, and new vertices generated.

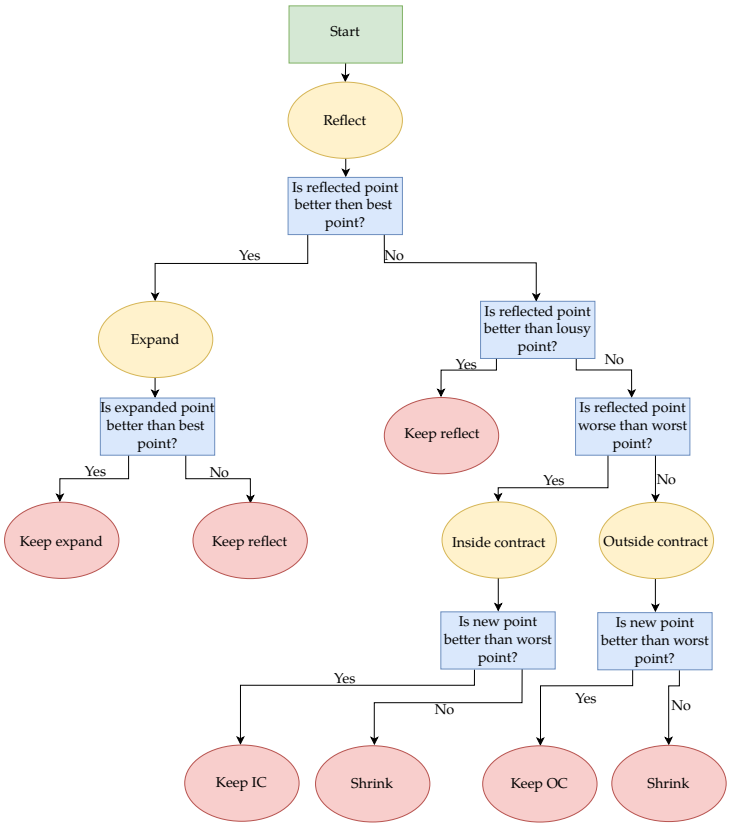

Figure 1.5: *Nelder-Mead decision tree*

The other convergence criteria is the a check to see if the best point is 'good enough'. The current best point is compared to a pre-set fitness value. If the best point is better than the pre-set value then the algorithm terminates.

1.5 Validation

The NM method was coded in Fortran, so that it could be easily interfaced with the MCRT code developed as part of this thesis. To test that the method works as intended a number of trial functions were tested, see Table 1.1. This was achieved by selecting an initial simplex, and the method allowed to iterate until it converged. The results of this are shown in Fig. 1.6.

Name	Formula	Global Minumum
Sphere	$x^2 + y^2$	$f(0,0) = 0.$
Rosenbrock	$(a-x)^2 + b(y-x^2)^2$	$f(1,1) = 0.$
Ackely	$-20\exp\left[-0.2\sqrt{0.5\left(x^2+y^2\right)}\right] -$ $\exp\left[0.5\left(\cos 2\pi x + \cos 2\pi y\right)\right] + e + 20$	$f(0,0) = 0.$
Himmelblau's	$(x^2 + y - 11)^2 + (x + y^2 - 7)^2$	$f(3,2) = 0.,$ $f(-2.805118, 3.131312) = 0.,$ $f(-3.779310, -3.283186) = 0.,$ $f(3.584428, -1.848126) = 0.$

Table 1.1: *Table of standard test functions for numerical optimisation.*

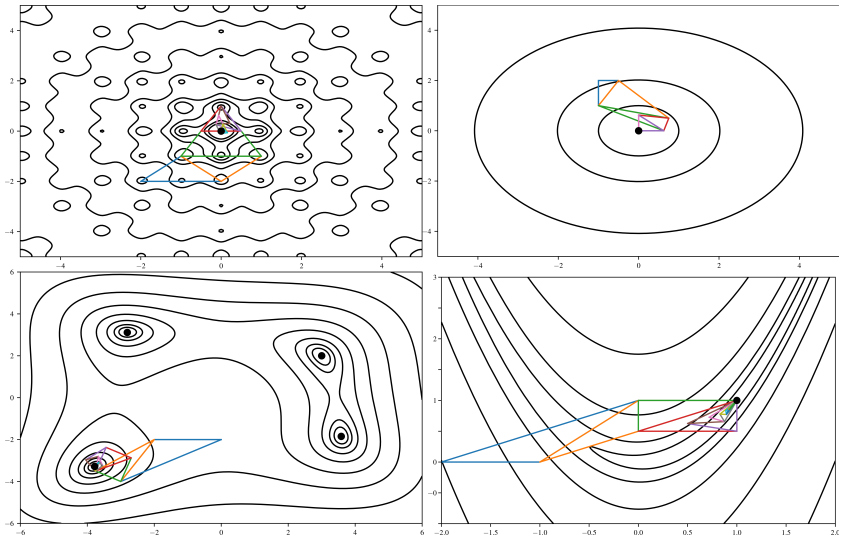

Figure 1.6: *Contour plots of test functions with Nelder-Mead simplexes over plotted. Top left is the Ackely function, top right is the sphere function, bottom left is the Himmelblau's function, and the bottom right is the Rosenbrock function. Blue simplex is the initial simplex, and the large black dots represent the Global minima.*

Some of these functions (Sphere, and Rosenbrock's) can also be extended to arbitrary dimensions. These functions were used to check that the NM method works as intended in these higher dimensions where the NM method will primarily be used in this thesis.

To ensure that the NM method can be used to find the unknown concentrations of the autoflurophores, we test the method with a known model. This model consists of three different fluorophores: NADH (nicotinamide adenine dinucleotide), FAD (flavin adenine dinucleotide), and a fictitious fluorophore that has similar properties to NADH and tyrosine, such that the excitation spectrum is that of NADH and the emission spectrum is that of tyrosine. The three fluorophores are distributed in the stratum corenum (NADH), epidermis (FAD), and the papillary dermis (fictitious). The concentration in these layers is such that the bulk optical properties are not affected: NADH has a concentration of 1.05 μM, FAD 0.525 mM, and the fictitious fluorophore has a concentration of 0.125 mM. The fitness function chosen to check whether the NM method is converging is as:

$$fitness = \sum_{i=1}^{n} (x_i - m_i)^2 \tag{1.16}$$

Where x_i is a data point at a wavelength λ_i produced by the MCRT, and m_i is a data point in the model at a wavelength λ_i.

As many models need to be run in order to determine whether a global maxima has been reached using the NM method and that the fluorophore concentration is low, means that many packets need to be run to achieve a good single to noise ratio. These two constraints result in a computational load that is infeasible to run. Therefore the MCRT algorithm has to be computationally efficient in order to arrive at an answer within a reasonable time. To this end the 3D skin model is shrunk to a 1D model so that the optical integration routine can efficiently move the photon through the simulated medium. The optical properties of the incident wavelength are also stored so that when a new photon is started the optical properties can easily be adjusted without need for any calculation. Finally a filter is employed on the output fluorescence spectrum to smooth the noise out. The filter used is a SavitzkyGolay filter. This filter fits multiple low-degree polynomials to the subsets of the output, thus smoothing the data.

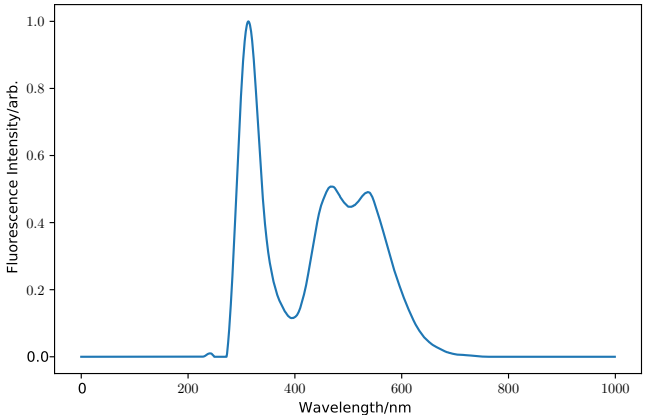

Figure 1.7: *Example of toy model for testing NM method. The three peaks correspond to the fictitious fluorophore, NADH, and FAD respectively.*

The above model is first run through the MCRT to get an output target spectrum. We then test the NM method for $n = 2$ and $n = 3$.

1.6 Results

Before running the NM method on the experimental data, the fluence of the input and fluorescence light is analyses alongside the location as a function of depth of the fluorescent light.

Figure 1.8 show the fluence as a function of depth for the indicent UV light. The figure shows that most of the incident light is contained within the top three layers, with little getting to the Reticular dermis, with none reaching the Hypodermis.

Figure 1.9 shows the fluence of detected fluorescent light (see Appendix B for discussion of how this is tracked.).

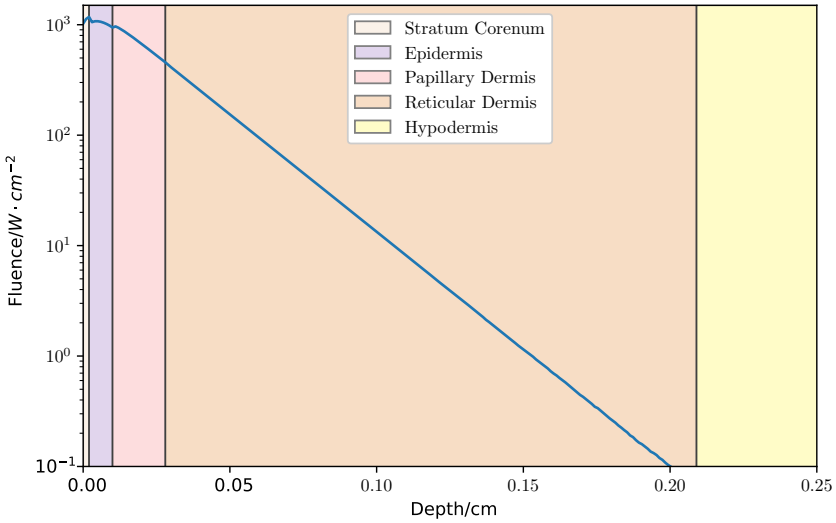

Figure 1.8: *Penetration of UV radiation as a function of depth.*

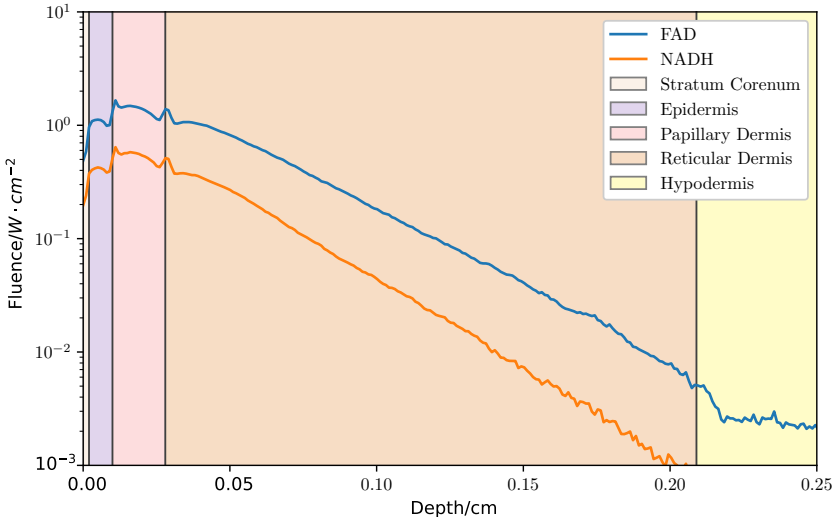

Figure 1.9: *Penetration of UV radiation as a function of depth.*

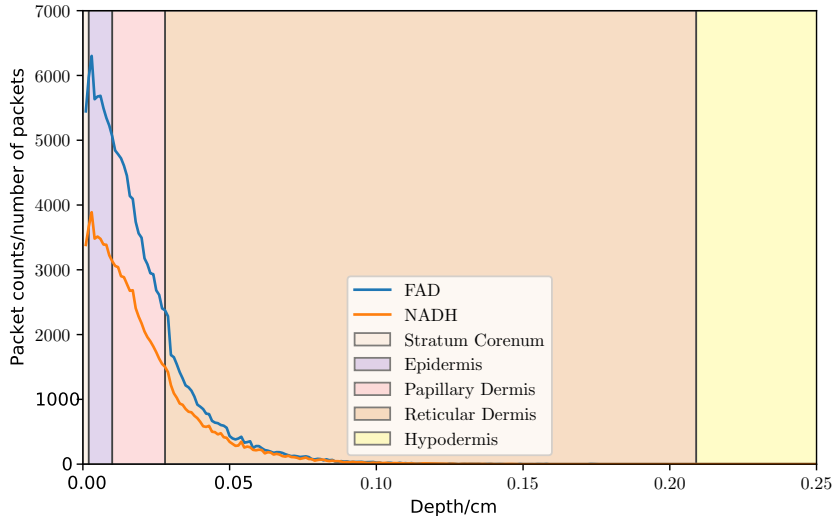

Figure 1.10: *Penetration of UV radiation as a function of depth.*

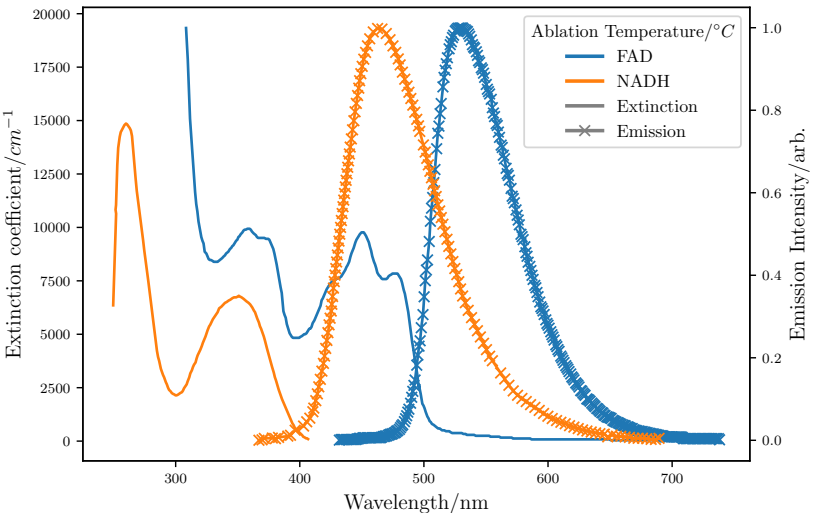

Figure 1.11: *Penetration of UV radiation as a function of depth.*

1.7 Discussion

1.8 Conclusion

We have presented out code, AmoebaMCRT, which combines the Nelder-Mead method and MCRT in order to determine the concentrations of naturally occurring fluorophores in human skin.

Appendices

Appendix A

Heat Equation Derivation

To derive the heat equation we consider the conversation of energy in a volume R, with a flux out, $\phi(x, y, z, t)$, and unit outer normal $\hat{\mathbf{n}}$. We need just the normal component of $\phi : \phi \cdot \hat{\mathbf{n}}$.

The rate of change of heat inside the volume R is equal to the heat generated inside the volume R plus the heat flowing in/out of the boundary surface:

$$\begin{array}{l}\text{Rate of change}\\ \text{of heat energy}\end{array} = \begin{array}{l}\text{Rate of heat}\\ \text{generation in}\\ \text{R}\end{array} + \begin{array}{l}\text{Rate of heat energy}\\ \text{flowing through bound-}\\ \text{ary surface}\end{array} \tag{A.1}$$

The total heat energy is:

$$e(x, y, z, t) = c(x, y, z) \cdot \rho(x, y, z) \cdot T(x, y, z, t) \tag{A.2}$$

and therefore the rate of change of heat energy is

$$\frac{d}{dt} \iiint_R e \; dV = \frac{d}{dt} \iiint_R c\rho T \; dV \tag{A.3}$$

We denote the heat generated inside the volume R as $Q(x, y, z, t)$:

$$\iiint_R Q \; dV \tag{A.4}$$

and the rate of heat energy flowing through the boundary surface is:

$$- \iint_{\partial R} \phi \cdot \hat{\mathbf{n}} \; dS^{\ddagger} \tag{A.5}$$

Substituting Eqs. (A.3) to (A.5) into Eq. (A.1), yields:

$$\frac{\partial}{\partial t} \iiint_R c\rho T \; dV = - \iiint_R \phi \cdot \hat{\mathbf{n}} \; dV + \iiint_R Q \; dV \tag{A.6}$$

Using the divergence theorem, and simplifying gives:

[‡]This is negative as outward flow ϕ is positive, but the flow would result in a reduction of energy.

$$\frac{\partial}{\partial t}\iiint_R c\rho T \; dV = -\iiint_R \nabla \cdot \phi \; dV + \iiint_R Q \; dV \tag{A.7}$$

$$\iiint_R \left[c\rho \frac{\partial}{\partial t} T + \nabla \cdot \phi - Q \right] dV = 0 \tag{A.8}$$

Which holds for an arbitrary R, thus:

$$c\rho \frac{\partial}{\partial t} T = -\nabla \cdot \phi + Q \tag{A.9}$$

Using Fourier's law of heat conduction, which states that the local heat flux density, ϕ, is proportional to the negative local temperature gradient. The proportionality constant being equal to the thermal conductivity, κ:

$$\phi(x, y, z, t) = \kappa(x, y, z) \nabla T(x, y, z, t) \tag{A.10}$$

Substituting Eq. (A.10) into Eq. (A.9) yields the heat equation:

$$c\rho \frac{\partial}{\partial t} T = \nabla \cdot (\kappa \nabla T) + Q \tag{A.11}$$

Which can be simplified into the homogeneous medium heat equation with the following assumptions: Q=0 and κ, ρ, *and* c are constant, and $\alpha = \frac{\kappa}{c\rho}$

$$\frac{\partial T}{\partial t} = \alpha \nabla^2 T \tag{A.12}$$

Appendix B

Detected Light Fluence Tracking Method

Most the fluence graphs presented in this thesis shows the fluence of the incident light throughout the simulated medium. However, there are problems where tracking the fluence of the detected light maybe useful, though this quantity is not straight forward to track. The current method of tracking fluence, is to add pathlengths, calculated as the packet moves from voxel to voxel to a 3D array. This method obviously cannot determine which packet will be detected before the packet is detected, therefore a new method must be devised. This new method tracks the coordinates, direction vectors, random optical distance and fluorescent source of the packet using a stack. A stack is a commonly used abstract data structure, and is a collection of elements. In this case the elements are the coordinates, direction vectors, optical distance and fluorescent source. A stack has two main operations, pop and push. The push operation adds a new element to the collection, and the pop operation removes the most recently added element from the collection. This is known as last in first out (LIFO). Figure B.1 shows these two operations in action.

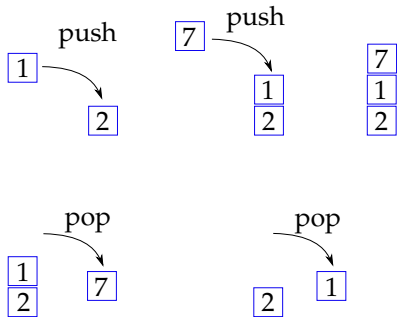

Figure B.1: *Example of the push and pop operation on a stack. The first operation add the integer 2 to the stack. The second operation push 7 to the stack. The last operation pops the 7 from the stack.*

The progress of each packets is pushed onto the stack, as it is propagated through the simulated medium. As mentioned above the packets coordinates, direction vectors, optical depth, and fluorescent source are the quantities pushed to the stack. These quantities are pushed to stack every time an interaction event occurs. When a packet is terminated, either via absorption

or it leaving the medium, the packets details are removed from the stack. This occurs unless the packet is detected. If the packet is detected then the information remains on the stack. This whole process repeats until all the packets have been run. Once all the packets have been run, the packets are "replayed". This is achieved by popping the information off the stack and passed to the inttau2 routine. The packet is the propagated again, this time recording the fluence as done in most of the chapters in this thesis.

Bibliography

[1] Steven L Jacques. Optical properties of biological tissues: a review. *Physics in Medicine & Biology*, 58(11):R37, 2013.